

Energy Spectrum of Fast Second Order Fermi Accelerators as Sources of Ultra-High-Energy Cosmic Rays

Tobias Winchen^{a,*}, Stijn Buitink^a

^a *Vrije Universiteit Brussel, Pleinlaan 2, 1050 Brussels, Belgium*

Abstract

Stochastic acceleration of cosmic rays in second order Fermi processes is usually considered too slow to reach ultra-high energies, except in specific cases. In this paper we present the energy spectrum obtained from second order Fermi acceleration in highly turbulent magnetic fields as e.g. found in the outskirts of AGN jets in situations where it can be sufficiently fast to accelerate particles to the highest observed energies. We parametrize the resulting non-power-law spectra and show that these can describe the cosmic ray energy spectrum and mass-composition data at the highest energies if propagation effects are taken into account.

Keywords: High energy cosmic rays, UHECR, Acceleration of particles, Fermi-acceleration, Cosmic ray sources, Spectrum, Hillas' Plot

1. Introduction

Cosmic rays are observed with energies from approximately 10 GeV up to energies above 100 EeV with a distribution commonly parametrized as a power-law. The spectral index of the power-law changes at a few certain energies, in particular the ‘knee’ at approximately 1×10^{15} eV and the ‘ankle’ at approx. 5×10^{18} eV. Beyond approx. 4×10^{19} eV the flux is strongly suppressed compared to a simple power-law. The definite origins of cosmic rays and the spectral features knee, ankle, and cut-off are still unknown, but in the prevailing models cosmic rays with the highest energies are of extragalactic origin while cosmic rays with the lowest energies are accelerated in sources within the galaxy (e.g. [1]).

It is typically assumed that the energy spectrum of the cosmic rays at their sources has also to be a single power-law $dN/dE \propto E^{-\gamma}$, maybe with some cut-off at high energies, in order to obtain the power-law observed at Earth (e.g. [2]). A power-law is the natural result of a stochastic acceleration of particles, when in every acceleration cycle a constant fraction of particles is lost. Notably, acceleration in relativistic shocks via the so called first order Fermi mechanism is considered as an acceleration mechanism that generates a power-law. In the shock acceleration model, a particle traverses a shock front multiple times and is efficiently accelerated, as it gains energy in every cycle. However, this mechanism has some difficulties, as the particles have to return to the shock many

times which require special conditions in the shock environment, a high injection energy of the particles into the accelerating region, or multiple shocks [3, 4].

From first order Fermi acceleration in diffusive shocks, a soft spectral index of the injection power-law of $\gamma \geq 2$ is expected [5]. However, it has been recently recognized by the Pierre Auger Collaboration [6, 7] and others [8–10], that the spectrum and composition data at the highest energies can not be well described by sources with a power-law spectrum and a soft spectral index; instead, hard spectra with $\gamma < 1.5$, or even $\gamma < 0$ depending on the model for the infrared background, are required to fit the data with a single power-law.

These problems do not arise in the original ‘second order’ acceleration mechanism proposed by Fermi [11], where particles gain energy in collisions with magnetic clouds. Here energy losses are frequent due to tail-on collisions, the average energy gain per collision is only $\Delta E/E = \frac{4}{3}\beta^2$. For velocities of the scatter centers $\beta \ll 1$ this second order acceleration thus requires a large number of scatter events to significantly gain energy. With the originally considered low rate of scatters with slowly moving magnetic clouds at Galactic distances, the mechanism is thus not fast enough to reach the highest observed energies within the lifetime of the respective sources.

To reach the highest energies via second order Fermi acceleration nevertheless, a high velocity of the scatter centers and/or a low mean free path length between scatter events is required. In the relativistic limit $\beta \approx 1$ the second order mechanism becomes as efficient as the first order mechanism. This scenario has been discussed in the literature [12] in particular in the context of acceleration inside GRBs. In general it also yields a power-law emission spec-

*Corresponding author

Email address: tobias.winchen@rwth-aachen.de (Tobias Winchen)

trum.

Here we focus on the second case of scattering with a short mean free path. Such conditions may be found in turbulent magnetic fields; for example, scattering on Alfvén waves in the radio lobes of AGNs, and in particular Centaurus A, has been considered [13–15]. In this paper we will first discuss our simulations setup and the spectrum we obtain with it from second order Fermi accelerators. We will then use a parametrization of the acceleration spectrum to fit observational data with the obtained acceleration spectrum taking propagation effects into account. The parameters obtained in the fit, the assumptions of the simulation as well as potential acceleration environments are then discussed before we draw our final conclusions.

2. Cosmic Ray Diffusion as Random Walk

The diffusive propagation of particles that scatter at irregularities $\frac{B}{\delta B}$ of magnetic fields with strength B , can be described as a random walk with step length $\lambda \propto D$ for diffusion coefficient D . The value of the diffusion coefficient D , its dependence of the energy of the particle, and the underlying principles of magnetic turbulences in astrophysical plasmas are a complex subject of ongoing intensive studies [e.g. 16].

A simplistic approach to diffusion of charged particles in magnetic fields is quasi-linear theory, where only slow evolution of the plasma is assumed [17]. Here the mean free path λ of a particle with energy E and charge Z in a field with turbulence spectrum $\frac{k}{k_{\min}}^{-q}$ is

$$\lambda = \left(\frac{B}{\delta B} \right)^2 (R_G k_{\min})^{1-q} R_G \equiv \lambda_0 \left(\frac{E}{1 \text{ EeV}} \frac{1}{Z} \right)^{2-q} \quad (1)$$

where $R_G = \frac{E}{BZ}$ is the gyro-radius of the particles [18]. This approximation for diffusive transport of particles with gyro-radius not larger than the correlation length of the field has been successfully used in several studies of particle acceleration and transport [e.g. 13, 19].

However, this formalism is too simplified to provide an accurate quantitative description of propagation in turbulent fields. In particular, turbulence is anisotropic [20] and scattering on small length scales is dominated by fast-modes instead of Alfvénic modes [21]. For particles with small gyroradius smaller than the turbulence injection scale of the magnetic field the propagation is dominated by fast super-diffusion [22].

Consequently the numerical value of the calculated diffusion coefficient for a given set of plasma parameters is not correct and also the dependency of the scatter frequency on the particle rigidity is not necessarily uniform over all scales as suggested by QLT. In particular the scatter frequency increases at low energies, eventually reaches a plateau or peak, and decreases again [23]. Nevertheless, the increase of the step length can be parametrised

by a power-law as is expected in some non-linear theories [24] and seen in simulations [25], at least above a certain threshold rigidity. Therefore, we use as simplified model for second order Fermi acceleration a random walk with a step length given by eq. 1 in our simulation and consider λ_0 and q free fit parameters. We further assume that particles are injected by a pre-accelerator above a threshold energy where these assumptions are valid.

3. Simulation

To simulate particle acceleration by magnetic scattering we follow a test-particle approach. Neglecting the back reaction of the particle on the magnetic field is valid here, because we are concerned only with the small fraction of cosmic rays at the highest energies. We demonstrate later that the energy transferred to UHECR from the field is much smaller than the energy transferred to radio emission in potential sources, thus justifying this approach.

We implemented the simulation as a dedicated module within the CRPropa framework [26]. The module scatters the particles into a random direction in the rest-frame of a scattering center moving with velocity β in the laboratory frame after propagating a distance d randomly chosen according to an exponential distribution with mean free-path λ according to eq. 1. We assume isotropic movements of the cosmic rays and scatter centers in the rest frame of the accelerating region. The distribution of angles θ between the direction of the particle and the scatter center is thus $dN/d\theta \propto 1 - \beta \cos \theta$. In every scatter event a random direction is chosen according to this distribution. As by this head-on collisions are more likely than tail-on collisions, the particle gains on average energy as predicted by second order Fermi acceleration.

The particles are injected with energy E_{inj} into the center of a spherical simulation volume with radius R , corresponding to a weak pre-acceleration e.g. in the inner parts of the AGN jet. Every particle propagates linearly until it is scattered as described above. We stop the simulation when the particle leaves the simulation volume or is decelerated below a lower energy threshold E_{low} . Injection energy and lower energy threshold are chosen as $E_{\text{inj}} = 100 \text{ TeV}$ and $E_{\text{low}} = 1 \text{ TeV}$ as in CRPropa currently only the highly relativistic case $E \gg m_0 c^2$ can be calculated. The simulation does not depend on the absolute scale of λ_0 and R , allowing us to investigate different values of their ratio λ_0/R , β , and q only. For acceleration of particles to energies much higher than the injection energy, the result is independent of the injection energy and thus on the spectrum of the pre-accelerator.

In figure 1 simulation results are shown for two choices of λ_0/R and for three choices of q covering a wide range of scaling of the step length with energy. In quasi linear theory these correspond to Kolmogorov turbulence ($q = 5/3$), Kraichnan turbulence ($q = 3/2$), and as an extreme case viscosity damping ($q = 1$) [27, 28]. However, in realistic models of turbulence the scaling parameter q can also

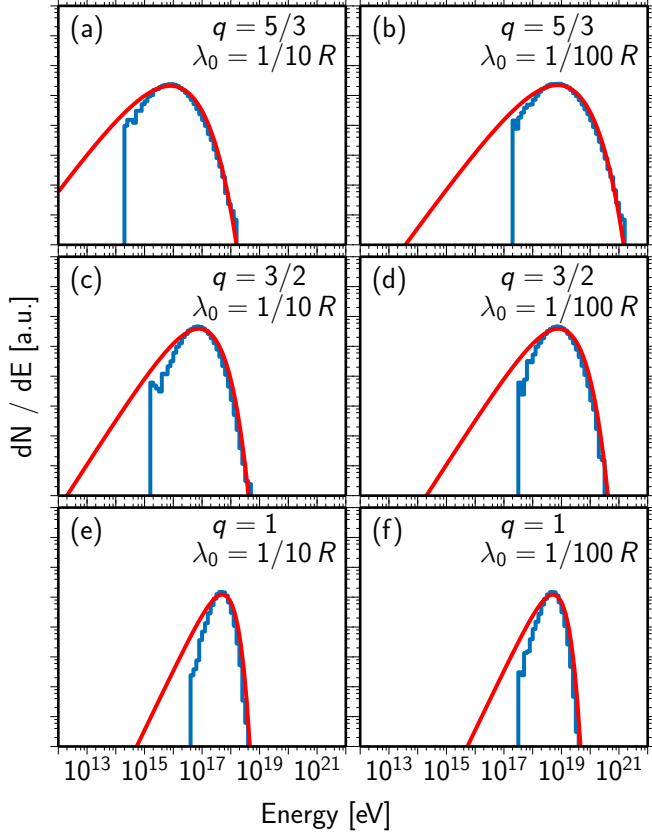


Figure 1: Emission spectra of the sources obtained from the simulation of second order Fermi acceleration of protons with different values for the mean free path length parameter λ_0 and the turbulence spectrum q with $\beta = 0.05$. The red line shows a fit of eq. 2 to the data.

assume different values depending on the plasma configuration. In particular, turbulence is anisotropic and $q = 5/3$ is for the perpendicular spectrum only while for the parallel spectrum $q = 2$ [29]. These examples assume thus the effective step length as discussed above.

As the particles are injected here in the center of the acceleration region, they cannot escape without being accelerated first because of their small mean-free path. This is different from e.g. shock acceleration where a fraction of particles is lost after each cycle. In the model discussed here, low energy particles can only escape from close to the border of the acceleration region, while particles at the highest energies can escape from anywhere in the accelerating region. This effectively suppresses the naively expected power-law in the regime $\lambda_0 \ll R$, and the source spectrum can be reasonably well described by a peaking distribution

$$\frac{dN}{dE} \propto E^{(3-q)} e^{-(E/E_0)^{(2-q)}} \quad (2)$$

which we found on phenomenological grounds only. For larger λ_0 , or λ independent of the energy, both not shown here, the source spectra develop a steep power-law tail. Here, we concentrate on the case where the power-law tail

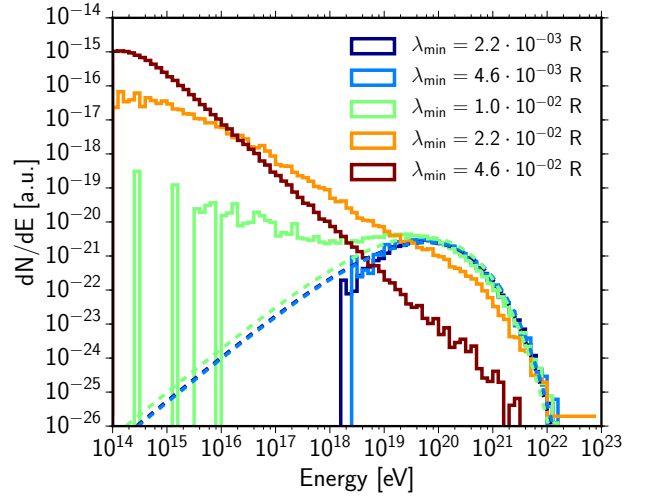


Figure 2: Source spectra with a fixed minimum step length λ_{\min} for $q = 5/3$, $\beta = 0.1$, and $\lambda_0 = \frac{1}{100} R$. Dashed lines correspond to a fit of eq. 2 to the simulated data above 30 EeV.

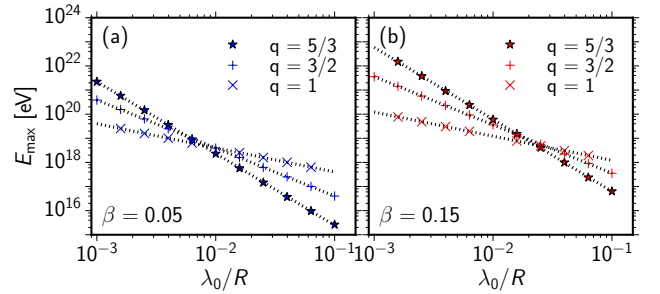


Figure 3: Maximum of the source spectra E_{\max} as function of the scatter length λ_0 for three choices of the turbulence spectrum q for (a) $\beta = 0.05$ and (b) $\beta = 0.15$. Colored markers are from a fit of eq. 2 to simulations as e.g. shown in figure 1; the dashed lines correspond to a power-law fit to the simulated points.

is negligible small, respectively the energy range close to E_0 .

From detailed simulations of diffusive propagation in magnetic fields it is known that a uniform scaling of the step length with a single power-law over the whole energy range as considered here is unrealistic. As suggested by simulations [e.g. 25], the step length is constant below a threshold rigidity corresponding to a Larmour radius $r_L \approx \frac{1}{10} L_{\max}$ with turbulence injection scale L_{\max} . The source spectra obtained in corresponding simulations with different choices of λ_{\min} are shown in figure 2. A minimum step length thus has no effect on the obtained spectrum shape as long as the minimum step length λ_{\min} is still small compared to R despite the transition. For larger λ_{\min} the spectrum transforms into a power-law with cut off that can be still described by the exponential in eq. 2.

For a given size of the accelerating region, the parameter E_0 of the distribution depends on the mean free path length λ_0 , the velocity of the scatter centers β , and the

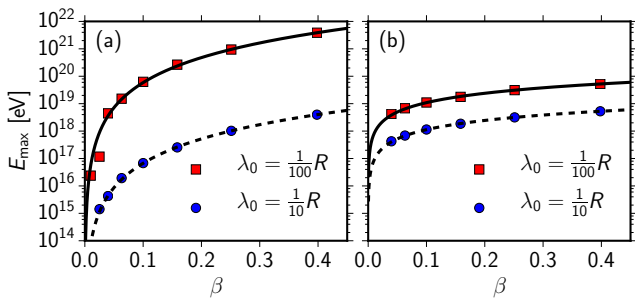


Figure 4: Maximum of the source spectra E_{\max} as function of the velocity of the scatter centers β for two choices of λ_0 for (a) $q = 5/3$ and (b) $q = 1$. Dashed and dotted lines correspond to a fit of $E_{\max} \propto \beta^a$.

spectral index q of the magnetic turbulence. From eq. 2 follows, that the position of the maximum of the distribution is given by

$$E_{\max} = \left(\frac{3-q}{2-q} \right)^{\frac{1}{2-q}} E_0. \quad (3)$$

The dependency of E_{\max} on λ_0 is shown in figure 3. We found no dependency of the shape of the spectrum or the maximum energy on the injection energy. The spectral shape is thus independent on the injection spectrum and thus the properties of the pre-accelerator as long as the energies reached by the pre-accelerator are not too high. A fit of a power-law $E_{\max} \propto \lambda_0^{\frac{1}{q-2}}$ to the simulation perfectly describes the dependency. This is consistent with eq. 1, as this relation implies a linear dependency of E_{\max} on the charge Z of the particles.

In figure 4 the dependency of E_{\max} on β is shown for two choices of λ_0 for $q = 5/3$ and $q = 1$. Points corresponds to a fit of eq. 2 to the simulation result and lines to a fit of $E_{\max} \propto \beta^a$ to the corresponding simulation sets. For $q = 5/3$ we found $a = 3.03 \pm 0.02$ and for $q = 1$ we found $a = 1.12 \pm 0.02$.

4. Fit

We fit the source spectrum given by eq. 2 to the observational data collected by the Pierre Auger Observatory [32] accounting for propagation effects using simulations of UHECR propagation with the CRPropa software [26]. We use the data on the flux of ultra-high energy cosmic rays [30] and the depth of shower maximum, X_{\max} , i.e. the depth at which the energy deposit of the electromagnetic cascade reaches its maximum [31]. The 1D-simulations used here include energy losses and production of secondaries from pion-production, photo-disintegration, and electron pair production in the cosmic microwave background and infrared background of particles from sources up to 3 Gpc. Energy losses by adiabatic expansion of the universe and energy losses and secondary production by

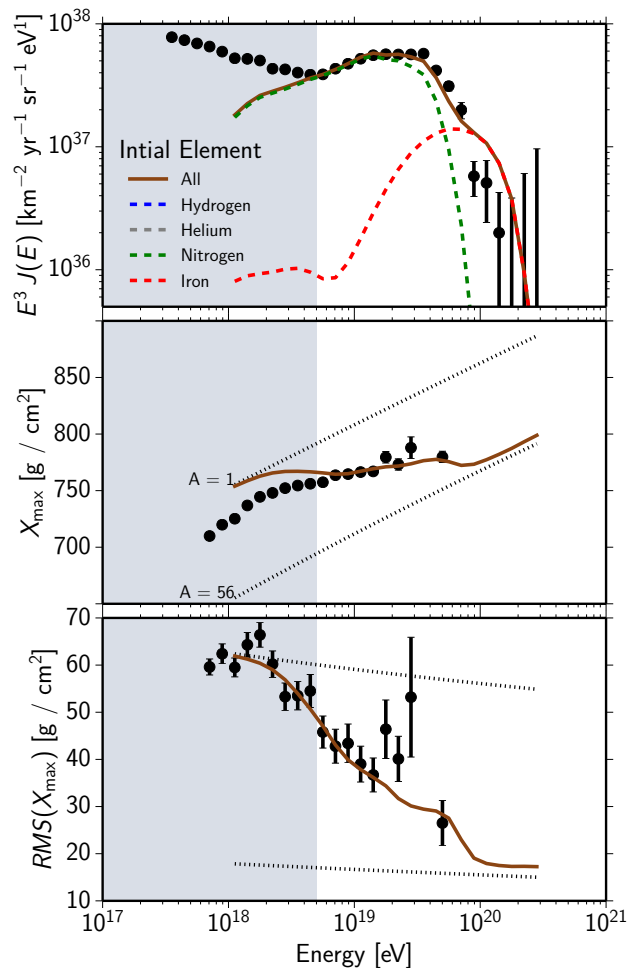


Figure 5: Two parameter fit of the model described here to the data of the energy spectrum [30] (top), and the mean (middle) and root-mean-square (bottom) of the X_{\max} distributions measured with the Pierre Auger Observatory [31]. For the spectrum fit the contribution from the individual initial elements are marked as dashed lines. The gray marked area is not included in the fit.

nuclear decay are included as well. As a model for the infrared background we consider here only Gilmore2012 [33] and as model for the nuclear cross-sections only TALYS [34]. An overview of the effects of these models on fits to cosmic ray data and simulation uncertainties is given in reference [35].

The fit-method used here is based on the method developed for the interpretation of the data of the Pierre Auger Observatory with power-law source spectra and an exponential cut-off [6, 7, 36]. To evaluate the effect of a source model on the observed cosmic rays, the energy and mass binned cosmic rays of a propagation simulation are re-weighted according to the source parameters. From the resulting weights for observed cosmic rays with energy and mass $(E, A)_i$ the spectrum and X_{\max} distributions are calculated. For the calculation of X_{\max} from $(E, A)_i$ we use the usual parametrization based on the Gumble dis-

tribution and EPOS-LHC [37] as the hadronic interaction model [38]. The optimum set of source parameters is obtained by maximizing the likelihood of the observations using a Markov chain Monte Carlo code [39]. Differently from the original approach, here we use a Gaussian-based likelihood for the mean and RMS of the X_{\max} distribution.

The best fit is obtained for $\log_{10}(E_{\max}/\text{eV}/Z) = 18.21 \pm 0.02$ and $q = 1.29 \pm 0.02$. With this fitting procedure, individual Markov Chains converge to different values for the individual element fractions while the values for q and E_{\max} are stable as indicated by a good Gelman-Rubin [40] statistic. The individual chains converge to different values for the individual elements, but the ratio of the Iron to Nitrogen fraction is well constrained in all Markov Chains to $f_{\text{Fe}}/f_{\text{N}} = (5.6 \pm 0.7) \cdot 10^{-4}$, and the values for Hydrogen and Helium are almost arbitrary due to the low maximum rigidity obtained in the fit. With these parameters, the expected values of the observables are shown together with the data in figure 5. For this four parameter fit to 36 data points we obtain a goodness-of-fit $\chi^2/\text{dof} = 58.8/32$.

5. Discussion

5.1. Fit

The model presented here fits the data approximately as well as fits assuming power-laws [6, 7]. This is not surprising, as from a mere technical point of view the spectrum proposed here is an inverted power-law with spectral index limited to $-2 \leq \gamma \leq -\frac{4}{3}$ and a slightly modified exponential cut off; results with $\gamma \leq 0$ have already been reported from fits of power-laws [6]. However, in the scenario as discussed here, this previously surprising parameter range is a natural consequence of the acceleration mechanism. The particular shape of the cut-off reduces the degeneracy between the parameters faced in fitting conventional power-law models. In particular, the cut-off expected here hardens the end of the spectrum compared to a naive exponential or broken-exponential cut-off; only for $q = 1$ the shape of the cut-off is identical to the common exponential cut-off. Consequently, the data above 5 EeV can be described with heavy primaries only and the fit becomes insensitive to the abundances of lighter elements.

Here we have considered only four elements, Hydrogen, Helium, Nitrogen, and Iron, where Nitrogen acts as a proxy for all elements with $2 < Z < 26$. Including more individual heavy elements in the fit will reduce the parameter E_{\max} further, as it allows a better description of the cut-off consistent with the ‘disappointing model’ [41]. The sources of extragalactic cosmic rays thus do not need to be surprisingly metal-rich as implied by power-law fits [42]. One can further speculate, that thus in this model the extragalactic sources of UHECR are also the origin of the strong light component below the ankle that have been recently measured [43, 44]. In addition to the inclusion of more elements, a detailed investigation of this requires the extension of the fit regime to lower energies and the

inclusion of Galactic models in the fashion of [45] and is beyond the scope of this paper.

5.2. Simulation

The approximation of diffusion in our simulation and the corresponding parametrizations are motivated by quasi-linear theory. QLT is based on the regime where the gyro-radius of the particle is not larger than the coherence length Λ of the field [17, 19]. The correlation length Λ of a turbulent magnetic field with energy distribution following a power-law with index q between length-scales L_{\min} and L_{\max} is defined as $\Lambda = \frac{1}{2} L_{\max} \frac{q-1}{q} \frac{(1-L_{\min}/L_{\max})^q}{1-(L_{\min}/L_{\max})^{q-1}}$. For $q > 1$ and $L_{\min}/L_{\max} \rightarrow 0$ we get $\Lambda = \frac{1}{2} L_{\max} \frac{q-1}{q}$; For $q \rightarrow 1$ we get a lower bound for the coherence length $\Lambda > \frac{1}{2} L_{\max} \frac{1-L_{\min}/L_{\max}}{-\ln L_{\min}/L_{\max}}$ as function of the span of the turbulence scales. Assuming that the maximum turbulence scale is of the size of the accelerating region yields that even for the extreme case $q = 1$ quasi-linear theory is applicable if the turbulence scales spans only two orders of magnitude and the accelerator is approximately ten-times larger than the gyro-radius. The constraints on L_{\min}/L_{\max} are greatly relaxed for $q = 5/3$, $q = 3/2$, or $q = 1.3$ corresponding to the best fit to the Auger data as obtained in this work. However, QLT does not account for several scattering processes likely found in realistic plasmas and may dominate particle propagation [e.g. 21, 22]. Nevertheless, an increase of the step length parametrised by a power law as used in our simulation also expected in at least some non-linear theories [24] and seen in simulations [25], at least above a certain threshold rigidity. Quantitative conclusions from the fit-result on the properties of the accelerator are thus not straight forward and require much ore detailed modelling of the acceleration environment.

By using a test particle approach for the simulations, we implicitly assumed that only a small portion of energy stored in the turbulent field is transferred to UHECR, because otherwise the turbulence spectrum is modified by collision-less damping, which would alter the spectrum of cosmic rays. However, as the spectrum from our acceleration mechanism is peaking and not a wide power-law, the energetics are here not dominated by the low-energy cosmic rays. This reduces the energetic constraints in this mechanism compared to mechanisms predicting a power-law. To obtain a conservative estimate, we attribute the UHECR flux to originate only from a single source in $D = 50$ Mpc distance, yielding a cosmic ray luminosity of $L_{CR} \approx 6 \times 10^{42} \text{ erg s}^{-1}$ for the best fit parameters and assuming iron primaries only. Thus even if only a single source accounts for the flux of UHECR, the energy transferred from the magnetic field to cosmic rays is much less than the energy transferred to radio emission in e.g. AGNs as sources. In case of multiple sources, the energy transferred to UHECR in a single source is much smaller.

Within the simulations we assume a constant, scale independent velocity of the scatter centers. However, due to

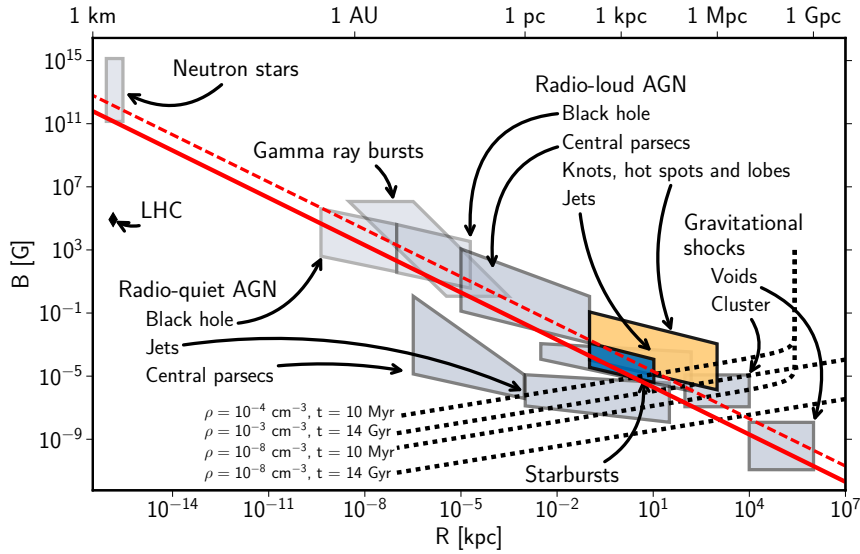


Figure 6: Possible accelerators for UHECR following an idea of Hillas’ [46], based on data published in reference [47]. The solid red line marks the gyro-radius R_G of an iron particle with 260 EeV, the red-dashed line $10R_G$. The black dotted lines correspond to time constraints following eq. 4 with maximum time t and density ρ as indicated left of the respective lines. The parameterspace below the respective lines is excluded.

energy cascading the velocity of the scatter centers may be reduced at low energies reducing the efficiency of this acceleration mechanism and thus sets an additional requirement to the pre-accelerator. Furthermore, we neglected any energy losses in particular by interaction with background photon fields in the source environments, as our simulations do not account correctly for the acceleration time due to the simplistic parametrization of the diffusion tensor.

5.3. Source Candidates

Following an idea of Hillas’, potential sources can be discussed in terms of the maximum achievable energy given their size and magnetic field strength. The source spectrum obtained here contains a natural cut-off beyond E_{\max} . However, the spectrum cannot continue indefinitely with exponential decay only as an absolute limiting energy E_{\lim} is given by the largest possible gyro-radius of the particles in the respective magnetic field. Here we can safely use $E_{\lim} \approx 10E_{\max}$ or $E_{\lim} = 260 \text{ EeV}$ for Iron nuclei consistent with observations. The classical constraint that the size of the accelerator has to be larger than the gyro-radius of the particles [46] provides thus not a severe constraint here and leaves in particular radio-loud AGN, starbursts and turbulence induced by gravitational shocks [47] as possible sources with this acceleration mechanism as indicated in figure 6.

The main argument against second order Fermi acceleration is commonly the required acceleration time. A rough upper limit for the acceleration time with second

order Fermi acceleration is

$$t_{\text{acc}} = 50 \left(\frac{\beta}{7 \times 10^{-4}} \right)^{-2} \left(\frac{R}{10 \text{ kpc}} \right)^{\frac{2}{3}} \left(\frac{E}{10^{19} \text{ eV}} \right)^{\frac{1}{3}} \text{ Gyr}, \quad (4)$$

assuming again that the maximum length-scale of the turbulence is the size of the accelerator [13]. As via the Alfvén velocity $\beta \propto \frac{B}{\sqrt{\rho P}}$ the acceleration time depends on the strength of the magnetic field B , eq. 4 can be used to constrain possible accelerators in a Hillas’ plot given their lifetime and plasma density ρP . In general, the acceleration mechanism thus selects large low-density environments. The largest low-density environments for considered UHECR acceleration are plasmas in clusters and voids with turbulence induced by gravitational shocks. Assuming a lifetime of 14 Gyr and densities of 10^{-3} cm^{-3} as inter-cluster density respectively 10^{-8} cm^{-3} for voids as extreme values [48], we can exclude turbulences induced by gravitational shocks as candidates for this mechanism. Radio lobes of AGNs as well as superwinds of starburst galaxies have a lifetime of more than 10^7 yr . If we assume a density below 10^{-4} cm^{-3} for the jets and lobes of radio-loud AGNs as well as superwinds emitted by starburst galaxies, both classes remain possible acceleration sites for this scenario as indicated in figure 6. This is consistent with similar estimates by Hillas [46].

Here of course we require that the turbulence spectrum covers large enough scales for the acceleration process. The highest energies can thus not be reached by this mechanism in the inner parts of AGN. Also, if the turbulence scale in the superwind of starbursts is much lower than their size, corresponding e.g. a ten times tighter constraint

on the gyro radius, only few starburst galaxies would provide the required conditions. However, this is no problem for potential acceleration in the radiolobes of AGN.

Both remaining candidate classes also fulfill the luminosity requirement [15, 49], that for any UHECR source $L > 10^{45} \left(\frac{E/Z}{10^{20} \text{ eV}} \right)^2 \text{ erg s}^{-1}$, which for the iron nuclei as above reads $L > 1 \times 10^{43} \text{ erg s}^{-1}$. With abundances of about 10^{-4} Mpc^{-3} both classes are furthermore consistent with observational bounds on UHECR [50, 51] and neutrino sources [52] as resulting from the low levels of anisotropy in the respective arrival directions.

6. Conclusion

The acceleration mechanism outlined here suggests the following picture as a potential scenario for the origin of UHECR. Cosmic-ray particles are first pre-accelerated in the inner parts of astronomical objects as potentially AGNs or starburst Galaxies (c.f. [53]) to an intermediate energy above the dissipation scale of the surrounding magnetic field in the AGN radiolobes respectively superwind of the starburst galaxies. In a second step the highest energies are then reached via the second order Fermi mechanism resulting in a peaking emission spectrum and not the commonly expected power-law. In contrast to interpretations of the data with power-laws as produced by shock acceleration, the best fitting parameters of the peaking source spectrum proposed here are not exceptional and do not imply an unexpected high abundance of heavy elements at the sources. It may thus be worth to reconsider the role of the usually disfavoured second-order Fermi mechanism for the acceleration of UHECR.

Acknowledgements

We gratefully acknowledge valuable comments to the manuscript from Roger Clay, Martin Erdmann, David Walz, and three anonymous referees. This research was funded by the European Research Council (ERC) under the European Union's Horizon 2020 research and innovation programme (grant agreement No 640130).

References

References

[1] K.-H. Kampert, P. Tinyakov, Cosmic rays from the ankle to the cutoff, *Comptes Rendus Physique* 15 (2014) 318–328. [arXiv:1405.0575](#), [doi:10.1016/j.crhy.2014.04.006](#).

[2] K. Kotera, A. V. Olinto, The astrophysics of ultrahigh energy cosmic rays, *Annual Review of Astronomy and Astrophysics* 49 (2011) 119–153. [arXiv:1101.4256](#), [doi:10.1146/annurev-astro-081710-102620](#).

[3] S. Colgate, Acceleration in astrophysics, *Physica Scripta T52* (1994) 96–105. [doi:10.1088/0031-8949/1994/T52/017](#).

[4] P. Blasi, Theoretical challenges in acceleration and transport of ultra high energy cosmic rays: A review, Invited Review Talk in UHECR2012 Symposium, CERN [arXiv:1208.1682](#).

[5] A. Marcowith, A. Bret, A. Bykov, M. E. Dieckman, L. O. Drury, B. Lembge, M. Lemoine, G. Morlino, G. Murphy, G. Pelletier, I. Plotnikov, B. Reville, M. Riquelme, L. Sironi, A. S. Novo, The microphysics of collisionless shock waves, *Reports on Progress in Physics* 79 (4) (2016) 046901.

[6] A. di Matteo for the Pierre Auger Collaboration, Combined fit of spectrum and composition data as measured by the pierre auger observatory, in: *Proceedings of the 34th International Cosmic Ray Conference*, 2015.

[7] A. Aab, et al., Combined fit of spectrum and composition data as measured by the Pierre Auger Observatory, *JCAP* 1704 (04) (2017) 038. [arXiv:1612.07155](#), [doi:10.1088/1475-7516/2017/04/038](#).

[8] D. Allard, N. Busca, G. Decerprit, A. V. Olinto, E. Parizot, Implications of the cosmic ray spectrum for the mass composition at the highest energies, *Journal of Cosmology and Astroparticle Physics* 10 (2008) 033. [arXiv:0805.4779](#).

[9] R. Aloisio, V. Berezhinsky, P. Blasi, Ultra high energy cosmic rays: implications of auger data for source spectra and chemical composition, *Journal of Cosmology and Astroparticle Physics* 2014 (10) (2014) 020.

[10] M. Unger, G. R. Farrar, L. A. Anchordoqui, Origin of the ankle in the ultrahigh energy cosmic ray spectrum, and of the extragalactic protons below it, *Phys. Rev. D* 92 (12) (2015) 123001. [arXiv:1505.02153](#), [doi:10.1103/PhysRevD.92.123001](#).

[11] E. Fermi, On the origin of the cosmic radiation, *Physical Review* 75 (1949) 1169.

[12] G. Pelletier, Cosmic ray acceleration and nonlinear relativistic wavefronts, *Astronomy and Astrophysics* 350 (1999) 705–718.

[13] S. O’Sullivan, B. Reville, A. M. Taylor, Stochastic particle acceleration in the lobes of giant radio galaxies, *Monthly Notices of the Royal Astronomical Society* 400 (2009) 248–257. [arXiv:0903.1259](#), [doi:10.1111/j.1365-2966.2009.15442.x](#).

[14] F. Fraschetti, On the acceleration of ultra-high-energy cosmic rays, *Philosophical Transactions of the Royal Society A: Mathematical, Physical and Engineering Sciences* 366 (1884) (2008) 4417–4428. [arXiv:0809.3057](#), [doi:10.1098/rsta.2008.0204](#).

[15] M. J. Hardcastle, C. C. Cheung, I. J. Feain, L. Stawarz, High-energy Particle Acceleration and Production of Ultra-high-energy Cosmic Rays in the Giant Lobes of Centaurus A, *Monthly Notices of the Royal Astronomical Society* 393 (2009) 1041–1053. [arXiv:0808.1593](#), [doi:10.1111/j.1365-2966.2008.14265.x](#).

[16] A. Lazarian, L. Vlahos, G. Kowal, H. Yan, A. Beresnyak, E. M. de Gouveia Dal Pino, Turbulence, Magnetic Reconnection in Turbulent Fluids and Energetic Particle Acceleration, *Space Science Reviews* 173 (2012) 557–622. [arXiv:1211.0008](#), [doi:10.1007/s11214-012-9936-7](#).

[17] R. Schlickeiser, Cosmic-Ray Transport and Acceleration. II. Cosmic Rays in Moving Cold Media with Application to Diffusive Shock Wave Acceleration, *The Astrophysical Journal* 336 (1989) 264. [doi:10.1086/167010](#).

[18] J. Scalo, B. G. Elmegreen, Interstellar turbulence ii: Implications and effects, *Annual Review of Astronomy and Astrophysics* 42 (1) (2004) 275–316. [doi:10.1146/annurev.astro.42.120403.143327](#).

[19] F. Casse, M. Lemoine, Pelletier, Transport of cosmic rays in chaotic magnetic fields 65.

[20] P. Goldreich, S. Sridhar, Toward a theory of interstellar turbulence. 2: Strong alfvénic turbulence, *Astrophysical Journal* 438 (1995) 763–775. [doi:10.1086/175121](#).

[21] H. Yan, A. Lazarian, Scattering of cosmic rays by magnetohydrodynamic interstellar turbulence, *Phys. Rev. Lett.* 89 (2002) 281102. [arXiv:astro-ph/0205285](#), [doi:10.1103/PhysRevLett.89.281102](#).

[22] A. Lazarian, H. Yan, Superdiffusion of Cosmic Rays: Implications for Cosmic Ray Acceleration, *Astrophys. J.* 784 (2014) 38. [arXiv:1308.3244](#), [doi:10.1088/0004-637X/784/1/38](#).

[23] H. Yan, A. Lazarian, Cosmic ray scattering and streaming in compressible magnetohydrodynamic turbulence, *Astrophys. J.* 614 (2004) 757–769. [arXiv:astro-ph/0408172](#), [doi:10.1086/](#)

- 423733.
- [24] A. Shalchi, *Nonlinear Cosmic Ray Diffusion Theories*, Springer, 2009. doi:10.1007/978-3-642-00309-7.
- [25] A. Beresnyak, H. Yan, A. Lazarian, Numerical study of cosmic ray diffusion in magnetohydrodynamic turbulence, *The Astrophysical Journal* 728 (1) (2011) 60.
- [26] R. Alves Batista, et al., Crpropa 3 - a public astrophysical simulation framework for propagating extraterrestrial ultra-high energy particles 05 (2016) 038. arXiv:1603.07142.
- [27] J. Cho, A. Lazarian, E. T. Vishniac, Ordinary and viscosity-damped magnetohydrodynamic turbulence, *The Astrophysical Journal* 595 (2) (2003) 812.
- [28] J. Cho, A. Lazarian, E. Vishniac, MHD Turbulence: Scaling Laws and Astrophysical Implications, 2003, pp. 56–100. arXiv:astro-ph/0205286.
- [29] A. Beresnyak, On the Parallel Spectrum in Magnetohydrodynamic Turbulence, *The Astrophysical Journal Letters* 801 (2015) L9. arXiv:1407.2613, doi:10.1088/2041-8205/801/1/L9.
- [30] I. V. for the Pierre Auger Collaboration, The flux of ultra-high energy cosmic rays after ten years of operation of the pierre auger observatory, in: *Proceedings of the 34th International Cosmic Ray Conference*, 2015.
- [31] A. Aab, et al., Depth of maximum of air-shower profiles at the Pierre Auger Observatory. I. Measurements at energies above $10^{17.8}$ eV, *Phys. Rev. D* 90 (2014) 122005. arXiv:1409.4809.
- [32] A. Aab, et al., The Pierre Auger Cosmic Ray Observatory, *Nucl. Instrum. Meth. A* 798 (2015) 172–213. arXiv:1502.01323, doi:10.1016/j.nima.2015.06.058.
- [33] R. C. Gilmore, R. S. Somerville, J. R. Primack, A. Domínguez, Semi-analytic modelling of the extragalactic background light and consequences for extragalactic gamma-ray spectra, *Monthly Notices of the Royal Astronomical Society* 422 (2012) 3189–3207. arXiv:1104.0671, doi:10.1111/j.1365-2966.2012.20841.x.
- [34] A. J. Koning, S. Hilaire, M. C. Duijvestijn, Talys: Comprehensive nuclear reaction modeling, *AIP Conference Proceedings* 769 (1) (2005) 1154–1159. doi:http://dx.doi.org/10.1063/1.1945212.
- [35] R. Alves Batista, D. Boncioli, A. di Matteo, A. van Vliet, D. Walz, Effects of uncertainties in simulations of extragalactic UHECR propagation, using CRPropa and SimProp, *JCAP* 1510 (10) (2015) 063. arXiv:1508.01824, doi:10.1088/1475-7516/2015/10/063.
- [36] D. Walz, Constraining models of the extragalactic cosmic-ray origin with the pierre auger observatory, Ph.D. thesis, RWTH Aachen University (2016).
- [37] K. Werner, I. Karpenko, T. Pierog, “ridge” in proton-proton scattering at 7 tev, *Phys. Rev. Lett.* 106 (2011) 122004. doi:10.1103/PhysRevLett.106.122004.
- [38] M. De Domenico, M. Settimo, S. Riggi, E. Bertin, Reinterpreting the development of extensive air showers initiated by nuclei and photons, *JCAP* 1307 (2013) 050. arXiv:1305.2331, doi:10.1088/1475-7516/2013/07/050.
- [39] A. Patil, D. Huard, C. Fonnesbeck, Pymc: Bayesian stochastic modelling in python, *Journal of Statistical Software* 35 (1) (2010) 1–81. doi:10.18637/jss.v035.i04.
- [40] A. Gelman, D. B. Rubin, Inference from iterative simulation using multiple sequences, *Statistical Science* 7 (4) (1992) pp. 457–472.
- [41] R. Aloisio, V. Berezhinsky, A. Gazizov, Ultra high energy cosmic rays: The disappointing model., *Astroparticle Physics* 34 (2011) 620–626. arXiv:0907.5194, doi:10.1016/j.astropartphys.2010.12.008.
- [42] D. Boncioli, A. di Matteo, A. Grillo, Surprises from extragalactic propagation of UHECRs, in: *Cosmic Ray International Seminar: The status and the future of the UHE Cosmic Ray Physics in the post LHC era (CRIS 2015)* Gallipoli, Italy, September 14–16, 2015, 2015. arXiv:1512.02314.
- [43] A. Porcelli, for the Pierre Auger Collaboration, Measurements of x_{\max} above 10^{17} ev with the fluorescence detector of the pierre auger observatory, in: *Proceedings of the 34th International Cosmic Ray Conference*, 2015.
- [44] S. Buitink, et al., A large light-mass component of cosmic rays at 1017-1017.5 electronvolts from radio observations, *Nature* 531 (7592) (2016) 70–73.
- [45] S. Thoudam, J. P. Rachen, A. van Vliet, A. Achterberg, S. Buitink, H. Falcke, J. R. Hrandel, Cosmic-ray energy spectrum and composition up to the ankle - the case for a second Galactic component, *Astronomy & Astrophysics* under review. arXiv:1605.03111.
- [46] A. M. Hillas, The origin of ultra-high-energy cosmic rays, *Annual Review of Astronomy and Astrophysics* 22 (1984) 425–44. doi:10.1146/annurev.aa.22.090184.002233.
- [47] K. V. Ptitsyna, S. V. Troitsky, Physical conditions in potential accelerators of ultra-high-energy cosmic rays: updated hillas plot and radiation-loss constraints, *Physics-Uspekhi* 53 (7) (2010) 691. arXiv:0808.0367, doi:10.3367/UFNe.0180.201007c.0723.
- [48] J. R. Peterson, A. C. Fabian, X-ray spectroscopy of cooling clusters, *Phys. Rept.* 427 (2006) 1–39. arXiv:astro-ph/0512549, doi:10.1016/j.physrep.2005.12.007.
- [49] M. Lemoine, E. Waxman, Anisotropy vs chemical composition at ultra-high energies, *JCAP* 11 (2009) 009. arXiv:0907.1354, doi:10.1088/1475-7516/2009/11/009.
- [50] P. Abreu, et al., Bounds on the density of sources of ultra-high energy cosmic rays from the Pierre Auger Observatory, *JCAP* 1305 (2013) 009. arXiv:1305.1576, doi:10.1088/1475-7516/2013/05/009.
- [51] A. Aab, et al., Search for patterns by combining cosmic-ray energy and arrival directions at the pierre auger observatory 75 (6) (2015) 269. arXiv:1410.0515, doi:10.1140/epjc/s10052-015-3471-0.
- [52] M. G. Aartsen, et al., All-sky search for time-integrated neutrino emission from astrophysical sources with 7 years of Ice-Cube data, *The Astrophysical Journal* under review. arXiv:1609.04981.
- [53] L. A. Anchordoqui, G. E. Romero, J. A. Combi, Heavy nuclei at the end of the cosmic ray spectrum?, *Physical Review D* 60 (1999) 103001. arXiv:astro-ph/9903145, doi:10.1103/PhysRevD.60.103001.